Photochemistry of benzene (C6H6) hydrogen cyanide (HCN) co-condensed ices part 1: A source of solid-state production of volatile nitrile compounds in Titan's stratosphere

J. Mouzay, K. Henry, I. Couturier-Tamburelli, G. Danger, N. Piétri, T. Chiavassa

Photochemistry of benzene (C_6H_6) hydrogen cyanide (HCN) co-condensed ices part 1: a source of solid-state production of volatile nitrile compounds in Titan's stratosphere

J. Mouzay[a], K. Henry, I. Couturier-Tamburelli[a], G. Danger[a,b,c], N. Piétri[a], T. Chiavassa[a]

[a] Aix-Marseille Université, CNRS, PIIM, UMR 7345, 13397 Marseille, France

[b] Institut Universitaire de France (IUF)

[c] Aix-Marseille Université, CNRS, CNES, LAM, UMR 7326, 13397 Marseille, France

Corresponding author : PIIM, Aix-Marseille Université, CNRS, UMR 7345, 13397 Marseille, France

E-mail address: isabelle.couturier@univ-amu.fr (I. Couturier-Tamburelli).

Abstract

Since 2015, during northern spring, a massive "noxious" stratospheric cloud has been detected at 250 km of altitude at the south pole of Titan, which persisted until the last targeted Cassini's flybys in July 2016. Its chemical composition seems to be the result of a co-condensation process of benzene and hydrogen cyanide in a 4:1 mixing ratio. Since, its altitude of detection allows to undergo long-UV solar radiations known to trigger photochemical aging processes, we experimentally simulated its evolution under stratospheric-like radiation conditions. The ice photo-processing (λ > 200 nm) led to the detection of nitriles by infrared spectroscopy such as acetonitrile (CH_3CN), benzonitrile (C_6H_5CN) as well as a partial identification of propionitrile (CH_3CH_2CN) and acrylonitrile (C_2H_3CN). Gas chromatography coupled to mass spectrometry (GC-MS) analyses of the volatile fraction released in the gas phase during the warming of the photo-processed ice have been confirmed by previous assignments and provided the detection of several other hydrocarbons ranging from C3 to C8. These experimental results are of prime interest in the context of the future Dragonfly mission. They provide a list of nitrile derivatives that can be produced from this stratospheric cloud. Indeed, they may contribute at the end to the organic layer that recovers Titan's surface and would be analyzed by the mass spectrometer (Dra-MS) of this space mission.

Introduction

Titan, Saturn's largest moon, has been probed for more than thirteen years by *Cassini-Huygens* space mission, with a hundred of targeted flybys. So far, Titan is the only satellite in

the solar system to possess a dense atmosphere highly reductive with a complex chemistry due to its N_2 and CH_4 composition, which ratio varies over the altitude (Niemann et al. 2010). In the upper part of the atmosphere, high energetic particles (electrons coming from Saturn's magnetosphere, X-rays, solar photons, …)(Coates et al. 2009; Galand et al. 2010; Waite et al. 2007; Yung et al. 1984) lead to the photo-dissociation of these main atmospheric constituents resulting in the formation of complex organic compounds (Coustenis et al., 2007; Cui et al., 2009; Imanaka & Smith, 2007; Magee et al., 2009; Samuelson et al., 1997; Waite et al., 2007). Since the first flyby of Titan by *Voyager 1*, numerous gaseous species are present in the surrounding gas phase (Coustenis et al. 1999; Hanel et al. 1981; Kunde et al. 1981; Samuelson et al. 1997), including hydrogen cyanide (HCN) (Coustenis et al. 2007; Hanel et al. 1981). Later, Composite Infrared Spectrometer instrument (CIRS) and Ion and Neutral Mass Spectrometer (INMS) of the Huygens probe extended of the molecules detected in the gas phase, and determined their relative abundance over the atmosphere (Coustenis et al. 2007; Cui et al. 2009; Koskinen et al. 2011). It was the case for benzene (C_6H_6) which was detected by ISO (Coustenis et al. 2003) and confirmed by Cassini CIRS/Huygens INMS (Coustenis et al. 2007; Waite et al. 2005).

At lower altitude, the decreasing stratospheric temperature profile allows organics to condense (Anderson et al., 2018, 2016; De Kok et al., 2007; Griffith et al., 2006; Khanna et al., 1987; Lavvas et al., 2011; Mayo & Samuelson, 2005; Samuelson et al., 2007, 1997; Samuelson & Mayo, 1991), resulting in the formation of ice particles (Lavvas et al. 2011, 2010). In this atmospheric region, the temperature variation lead to a chemical complexification of solid particles, which result from a coating with successive ice layers (Anderson et al., 2016). Theoretical models of the cloud microphysics and radiative transfer models have then established condensation profiles of gaseous molecules in the Titan's stratosphere for different seasons and regions (Anderson et al. 2018; Barth 2017; Lavvas et al. 2011). Besides, Cassini-Huygens space mission highlighted the formation of massive stratospheric ice clouds at low altitudes by ISS and CIRS instruments, at the southern pole, due to exceptional climatic conditions. Indeed, two years after the northern spring equinox in 2009, Titan's meridional circulation has been reversed. This inversion had the consequence of increasing the mixing ratios of trace organics in the southern hemisphere following a drastic cooling, with temperatures dropping under 120 K in the stratosphere at an altitude of 250 km(Achterberg et al. 2014; Coustenis et al. 2016). Vinatier et al. have shown that the 682 cm^{-1}

signature, observed below 300 km since 2013, is attributed for a part to the CH bending mode of benzene (C_6H_6) ice. More recently, in the same region during the late southern fall in 2015, Anderson et al. (2017) reported the detection of a massive cloud around 250 km of altitude with a 220 cm^{-1} far-infrared signature. This feature may result from the simultaneous condensation of benzene and hydrogen cyanide in a 4:1 ratio (Anderson et al. 2017, 2018).

FUV photons (Gudipati et al., 2013; Lavvas et al., 2008; Wilson, 2004) that reach the stratosphere can trigger photochemical reactions at these altitudes, representing the main process for the loss of molecules in this atmospheric layer. Besides, at 220 nm, the solar flux is estimated to be 1 x 10^{10} photons.cm^{-2}.s^{-1} at 200 km competing the one obtained at shorter wavelength in the highest atmospheric layers, which induces a complex gas-phase chemistry (Gudipati et al., 2013). This solar flux can also participate to the photochemical aging of Titan's stratospheric ice particles (Anderson et al. 2016). Anderson et al. (2016) showed also that the interaction of FUV solar photons with ice particles of HC_3N and HCN, like those detected in a northern stratospheric cloud, could lead to the solid-state formation of dicyanoacetylene (C_4N_2). The quantities of this photo-product were similar to those detected in the stratosphere. These observations led Anderson et al. (2016) to conclude that solid-phase C_4N_2 can be synthetized via a surface reactivity rather than a condensation at the surface of aerosols. Therefore, the photochemical evolution of Titan's stratospheric ice clouds could partially contribute to a change in chemical composition of the atmosphere. To account for these observations, we can rely on experimental simulations of FUV photolysis. These were carried out either on pure nitriles ices, i.e., hydrogen cyanide (HCN), acrylonitrile (C_3H_3N), propionitrile (C_3H_5N), cyanoacetylene (HC_3N),dicyanoacetylene (C_4N_2) (Couturier-Tamburelli et al., 2018a, 2018b, 2014; Gudipati et al., 2013) or on pure hydrocarbons ices with acetylene (C_2H_2) (Abplanalp et al. 2019) and benzene (C_6H_6) (Mouzay et al. 2021a). Moreover, with the help of GC-MS analyses, the formation of several kinds of volatile hydrocarbons, in particular aromatic derivatives such as toluene, ethylbenzene, xylenes and styrene were identified from the photochemistry of pure benzene ices under conditions relevant with Titan's stratospheric chemistry(Mouzay et al. 2021a,b). The formation of volatile nitrogen compounds was also identified by infrared spectroscopy (Toumi et al., 2016) and mass spectrometry (Couturier-Tamburelli et al. 2018b, Fleury et al. 2019) following the exposure of pure nitrile ices to FUV radiations, compatible with those reaching the stratosphere,. Except the experimental study of Pola et al. (2011) which emphasized, by GC-

MS analyses, the formation of nitriles derivatives from the photolysis (λ = 248 nm) of a gaseous C_6H_6/CH_3CN mixture, no other experiment was performed to understand the nitrogen-bearing species possibly generated from the photochemistry of C_6H_6:HCN ices in relevant Titan conditions. The resulting photoproducts could then sublimate enriching the gas phase, depending on the climatic conditions (if this HASP cloud is long-lived and in a steady state). Therefore, several experiments demonstrated the formation of diversified organics (hydrocarbons, aromatics, nitriles or amines) from N_2:CH_4 gas mixtures (Coll et al. 1999; Gautier et al. 2011; Hörst et al. 2018; Ramírez et al. 2005, 2001; Tran et al. 2005) in conditions simulating the photochemistry occurring from the stratopause to the highest atmospheric layers. However, the photochemistry of C_6H_6:HCN ices, relevant for Titan's stratospheric cloud chemistry is still lacking.

.

In this work, the role of the photochemical evolution of C_6H_6:HCN co-condensed ices is investigated in the energetic conditions of Titan's stratosphere. We particularly focus on the solid-state formation of volatile photo-products. Different ratios of C_6H_6:HCN ices were irradiated in low temperature conditions ,and their evolution was monitored by IR spectroscopy. The released compounds in the gas phase during the photo-processed ice warming were recovered and analyzed by gas chromatography coupled to mass spectrometry (GC-MS). These experiments allowed to determine if from such ices the low-energetic solar conditions of the stratosphere can lead to the formation of nitrogen derivative photo-products, from such ices.

1. Methods

1.1. Setup and formation of C_6H_6:HCN co-condensed ices

The description of the experimental setup, AHIIA, used for these experiments is detailed elsewhere (Abou Mrad, 2014). Gaseous benzene (for HPLC, assay ≥ 99.9%, from Sigma-Aldrich) was purified by several degassing steps with the help of nitrogen baths. HCN is synthesized by the thermal reaction of potassium cyanide (KCN) and an excess of stearic acid $CH_3(CH_2)_{16}COOH$ in a primary pumped vacuum line, as described in Gerakines et al. (2004). Benzene and hydrogen cyanide 4:1; 1:1 and 1:4 mixes have been prepared in a 1L-glass line. Gas mixtures were deposited on a polished copper surface, which temperature was controlled between 70 K to 300 K with a closed-cycle helium refrigerator and maintained

using a model 21 CTI cold head cryostat, a resistive heater, and a Lakeshore 331 temperature controller, within a high vacuum chamber (10^{-8} mbar). Each deposited gas sample corresponded to a quantity of about 20 µmol. The quantity of sample deposited was chosen to obtain an intensity inferior of 1 a. u. on IR spectra. The IR spectra were recorded in reflection-absorption mode in the mid-infrared region between 4000 and 600 cm^{-1} using a Bruker Tensor 27 Fourier transform infrared spectrometer with a DTGS detector. Each spectrum was averaged over 100 scans during photolysis experiments with a resolution of 1 cm^{-1}, except for the background averaged over 300 scans with the same resolution (Butsher et al. 2015).

Each co-condensed ice was deposited at 70 K, annealed to 105 K and followed by a cooling down to 70 K in order to increase the crystallization of C_6H_6 while preventing the desorption of both C_6H_6 and HCN (cf. supplementary information figure **S1**). Sublimation was supposed to occur at any temperature in a high vacuum chamber as compounds of the ice are in equilibrium with their vapor phase. Therefore, at 10^{-8} mbar in the chamber, this vapor can be continuously pumped, gradually causing the ice to sublimate. However, the lower is the temperature, the slower is the process. We have chosen to perform the experiments at 70 K, since a benzene/HCN ice starts to sublimate around 80 K in our experimental conditions (cf. supplementary information figure **S1**). Furthermore, this temperature provides trapping a maximum of photoproducts in the ice allowing their identifications. A drawback of this protocol is that some clusters of benzene or HCN can be formed during this protocol. (Hodyss et al. 2008, Lignell and Gudipati 2015) during the annealing to 105 K.

Photolysis was performed using an Oriel 500 W high-pressure mercury lamp (λ=200-2500 nm with discrete Hg lines in the UV-Vis region between 200 and 600 nm, where most of the photon flux (2.34 x 10^{16} photon.cm^{-2}.s^{-1}, ~13 mW.cm^{-2}) resides (Mouzay et al. 2021a, b) . The duration of the photolysis was chosen at 48 hrs to simulate a short sedimentation period of the co-condensed ices compatible with those expected in Titan's stratosphere (Gudipati et al. 2013). Moreover, using both a 1-D microphysical model (Lavvas, 2010, 2011) and a general circulation model (GCM) including microphysics aerosols (Larson et al. 2014), the residence time of aerosol in the Titan atmosphere has been estimated to be 395 Titanian years. According to the model of Larson et al., aerosols are supposed to spend most of their time in the lower atmosphere.

Considering a solar flux of ~10^{14} photons.cm^{-2}.s^{-1} at 100 km on Titan (Gudipati et al. 2013), the photons flux of the UV source employed is therefore 234 times more important than the one reaching the Titan's lower stratosphere. Consequently, 2 days of photolysis in the laboratory correspond to 468 days or 1.3 years on Titan which become 2.6 years by considering Titan's exposure to the sun during the day and the night. Furthermore, two other mandatory criteria related to experimental feasibility and chemical considerations have also led us to choose such a duration of irradiation: 1) because of benzene's weak electronic absorption at these wavelengths, the duration must be sufficiently long to observe spectral modifications using a low sensitivity in situ technique, i.e., IR spectroscopy: 2) to obtain only the formation of primary products.

After irradiation, the vacuum chamber was isolated from the pumping, and ice samples were warmed up to 300 K with the cryogenic system switched-off. Before this warming up, argon was added in the chamber to reach a total pressure of ~ 5 mbar (Abou Mrad et al. 2020) which optimizes the transfer of volatile organic compounds (VOC) from the chamber towards the pre-concentration loop. No modification on the photo-processed ice was observed with IR spectroscopy after Ar addition. The species sublimating from the ice were trapped over 16 h in a pre-concentration loop cooled in liquid nitrogen (77 K). This loop is part of the interface, named VAHIIA (Volatile Analyses from the Heating of Interstellar/cometary Ice Analogs) which connects vacuum chamber and GC-MS instrument. A detailed description of the interface is reported elsewhere (Abou Mrad et al. 2014, 2020). Subsequently, the pre-concentration loop was warmed and helium was added into the loop to reach a total pressure of 200 mbar which facilitates the sample transfer to the injection unit of the GC-MS (Abou Mrad et al. 2016, 2020). The injection unit ensures the online injection of the sample through a specific gas injection loop (500 µL) to the injector of the GC-MS instrument as described in the next section.

1.2.GC-MS conditions for sample analysis

The GC-MS analyses were performed on a ThermoFisher Trace 1310 gas chromatograph coupled to a ThermoFisher ITQ 900 MS ion trap, which has been modified for gaseous sample injection. A detailed description of the setup is described elsewhere (Abou Mrad et al. 2014). A volume of 500 µL of samples was injected into a split/splitless (SSL) injector kept at 300°C operating in split mode with a ratio of 10. The GC-MS injection loop

for gaseous samples is maintained at 110°C. Analytes were separated on a Rxi®-624Sil MS (60m x 0.25mm i.d. x 0.25 µm film thickness), using helium as carrier gas with a constant flow rate of 1 $mL.min^{-1}$. The initial temperature of the column was set at 45°C and hold for 3 min, followed by an increase of $5°C.min^{-1}$ to 150°C and then by $20°C.min^{-1}$ to 220°C hold for 2 min. The transfer line to the mass spectrometer was set to 250°C. The ion source temperature was set to 250°C and the maximum ion time in the trap is of 25 ms. The ion trap mass spectrometer worked with electronic impact as ionization mode (ionization energy of 70eV). The signal was collected with a full scan mode in the 15-300 u. mass range and a scan event time of 0.16 s. For these analyses, the GC has been modified with the implementation of a MicroJet Cryo-Trap MJT-1035E from Frontier Laboratories LTD on a Restek Rxi guard column (20cm x 0.25 mm i.d.) to enhance detection sensitivity as well as chromatographic resolution (Abou Mrad et al. 2020).

1.3.GC-MS peak identification methodology

The identification of VOC was performed by comparing retention time and mass spectrum of the sample chromatographic peaks with the ones of analytical standards which include hydrocarbons, aromatics and nitriles derivatives. Standards were pre-concentrated in the loop of the VAHIIA interface with the exact same protocol (Abou Mrad et al. 2014) than the one used to recover VOC from irradiated ices. The confirmation of identifications of hydrocarbon compounds was performed by comparing the mass spectrum of peaks detected from the $^{12}C_6H_6$:HCN experiment with the ones detected in a $^{12}C_6H_6$ experiment, already confirmed with $^{13}C_6H_6$ isotopic experiment (Mouzay et al. 2021b). For nitrogen compounds, we performed a C_6H_6:HCN^{15} experiment. Hence, in this last experiment, fragment that contain *x* N atom(s) will shift from *x* mass unity allowing to assess the number of nitrogen atom constituting the considered molecule.

I. Spectroscopic properties of C_6H_6:HCN ices

The interaction of benzene with hydrogen cyanide was studied theoretically (Mateus et al. 2011) and showed that linear or cyclic aggregates could be formed between benzene and hydrogen cyanide molecules (benzene:nHCN with $n \leq 4$). However, no spectroscopic information relative to these aggregates has been reported, to our knowledge. Therefore, to simulate different condensation scenarios that may occur in Titan's atmosphere depending on

the climatic conditions, we considered benzene/HCN ice ratios. Afterwards, the considered benzene (C_6H_6)/HCNice will be designated by its mixing ratio (1:1, 1:4 and 4:1) The gaseous mixture C_6H_6:HCN has been deposited at 70 K to prevent desorption of benzene and HCN at higher deposition temperatures. After the deposition a rapid annealing at 105 K was performed in order to maximize the crystalline state of the benzene in the ice. A cooling down to 70 K was then performed to limit the HCN desorption In figure **1,** the infrared spectra of C_6H_6:HCN ices in the 1:4, 1:1 and 4:1 ratios were compared to pure C_6H_6 and HCN ices, deposited with the exact same methodology. The $\nu_2 + \nu_{13} + \nu_{16}$ IR feature (which shape is not affected by the change of chemical environment) of benzene were normalized from the spectrum of the 1:4 ratio to the one of the 1:1 ratio. Similarly, the ν_1 IR feature of HCN in the 4:1 ratio was normalized to the one of the 1:1 ratio. Except a slight shift of band frequencies, due to the presence of HCN, the shape of benzene features in the 4:1 mix is similar to the one observed with the crystalline C_6H_6 ice (Mouzay et al. 2021a). Indeed, benzene is present in a crystalline form in this 4:1 ratio whereas in the 1:1 and 1:4 mixes, the benzene is amorphous. Hence, the increase of the HCN proportion in the mixtures induced a loss of organization of the benzene network preventing its crystallization. The complexation between C_6H_6 and HCN molecules also induces a shift of the ν_1 HCN mode toward high frequencies with respect to the same νCH absorption band of the HCN monomer. This shift can be up to 16 cm^{-1} in the 1:4 mixtures. Finally, we observe an additional band peaking is observed between 3200 and 3210 cm^{-1}. This band is not observed in the infrared spectrum of monomers and its position depend on the C_6H_6 and HCN ratios. This band is characteristic of aggregates formation between C_6H_6 and HCN. Wavenumbers of benzene and hydrogen cyanide vibrational modes in each ice ratio are listed in table **1.**

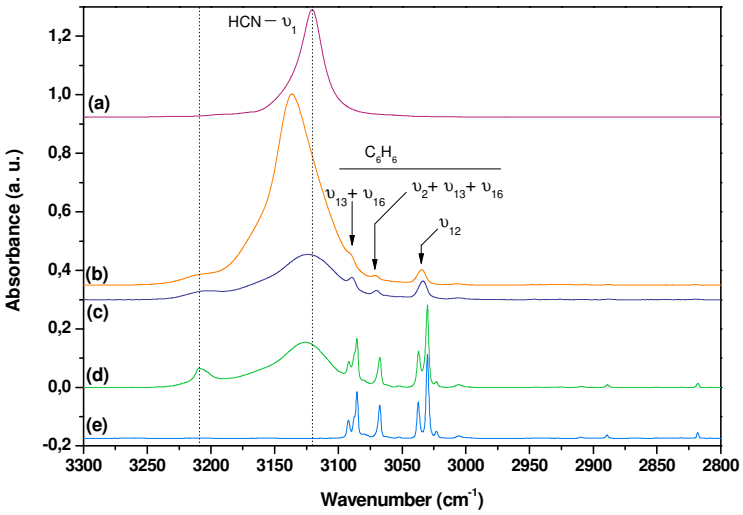

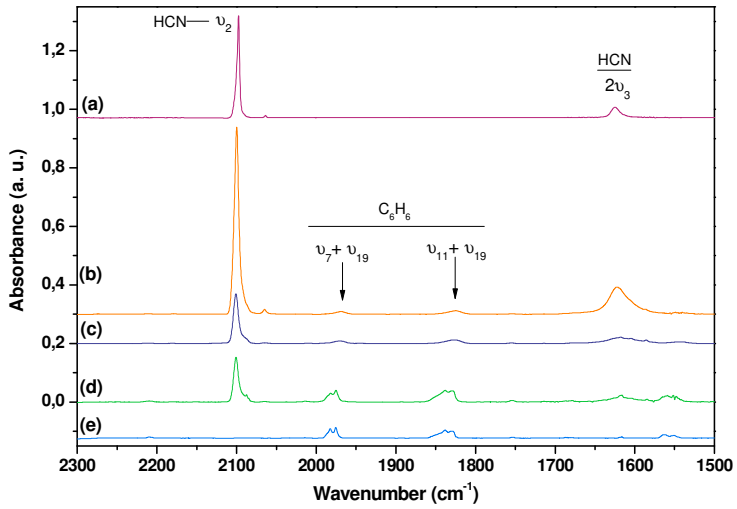

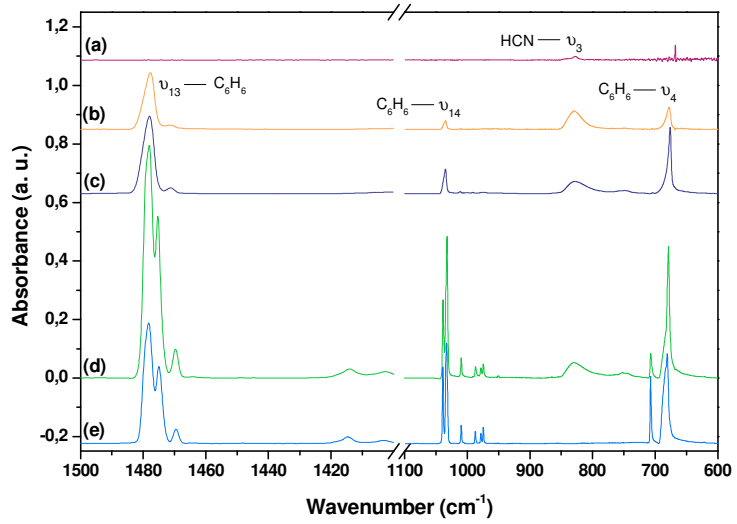

Figure **1** – Enlarged regions of IR spectra of ices deposited at 70 K annealed to 105 K and followed by a cooling down to 70 K: (a) pure crystalline HCN ice; C_6H_6:HCN co-condensed (b) ratio 1:4, (c) ratio 1:1, (d) ratio 4:1 ; (e) pure crystalline benzene ice

II. Investigating C_6H_6:HCN ices photochemistry under long-UV photons

The photochemistry of pure benzene or pure hydrogen cyanide ices in Titan's stratospheric-like conditions showed (Couturier-Tamburelli et al. 2018a, Mouzay et al. 2021a,b) that crystalline HCN ice is not photo-chemically active under mercury lamp radiations. Benzene ice demonstrated a weak photo-degradation rate, explained by the weak absorption of benzene in this wavelength range corresponding to singlet-singlet absorption ($^1B_{2u} \leftarrow {}^1A_{1g}$) or singlet-triplet absorptions ($^3E_{1u} \leftarrow {}^1A_{1g}$, $^3B_{2u} \leftarrow {}^1A_{1g}$) (Dawes et al. 2017).

To simulate the solar photons reaching Titan's stratosphere (Gudipati et al., 2013; Lavvas et al., 2008; Wilson, 2004), each C_6H_6:HCN ice was irradiated with a mercury lamp. Whatever the considered ratio, results are similar. Consequently, we focused on C_6H_6:HCN 4:1 ice since its composition simulates that of Titan's High Altitude Stratospheric Polar (HASP) cloud. Ices were irradiated during 48 hrs at 70 K after the annealing to 105 K. During the photolysis, a depletion of infrared bands of benzene and hydrogen cyanide infrared absorption bands are observed, visualized through negative bands on the subtraction spectra (figure **2**)**.** While a pure ice of HCN is not reactive in these conditions (Couturier-Tamburelli et al. 2018a), in the case of benzene/HCN ice, HCN reacts with photo chemically-activated benzene to form new nitrogen-bearing compounds. Furthermore, with the photolysis of the 4:1 ice, a photo-reactivity similar to that of pure benzene ice is observed (Mouzay et al. 2021a). Indeed, characteristic bands of benzene polymers are observed, as well as increase of amorphous benzene ones demonstrating an amorphization of the ice during the photolysis (cf. figure **3**). Finally, the absorption bands observed at 1341, 1078, 946, 898, 783 and 627 cm^{-1} coming from direct benzene photolysis could be assigned to fulvene molecule, one of benzene's valence isomers (Mouzay et al., 2021a, c) cf. figure **4**).

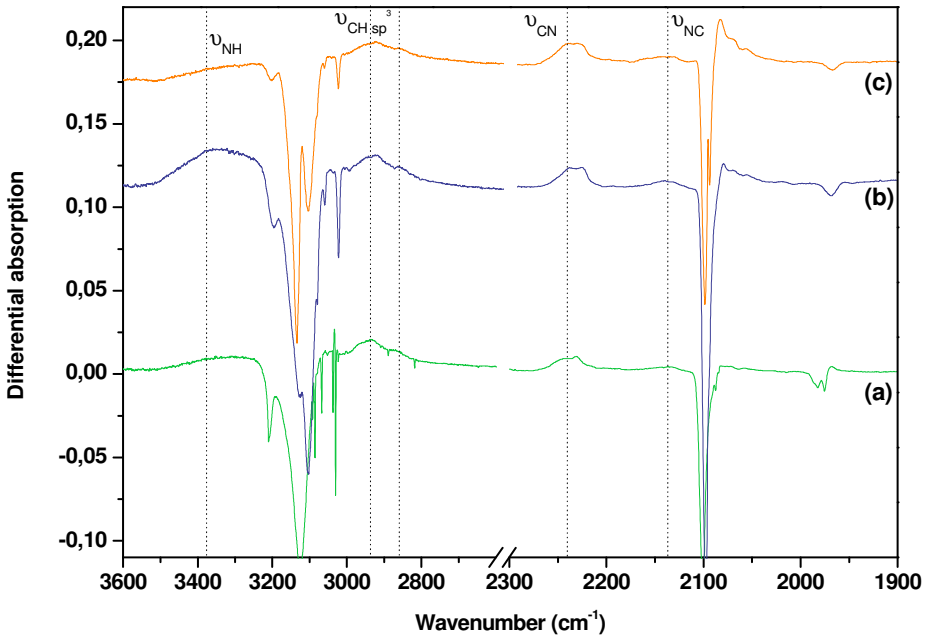

282

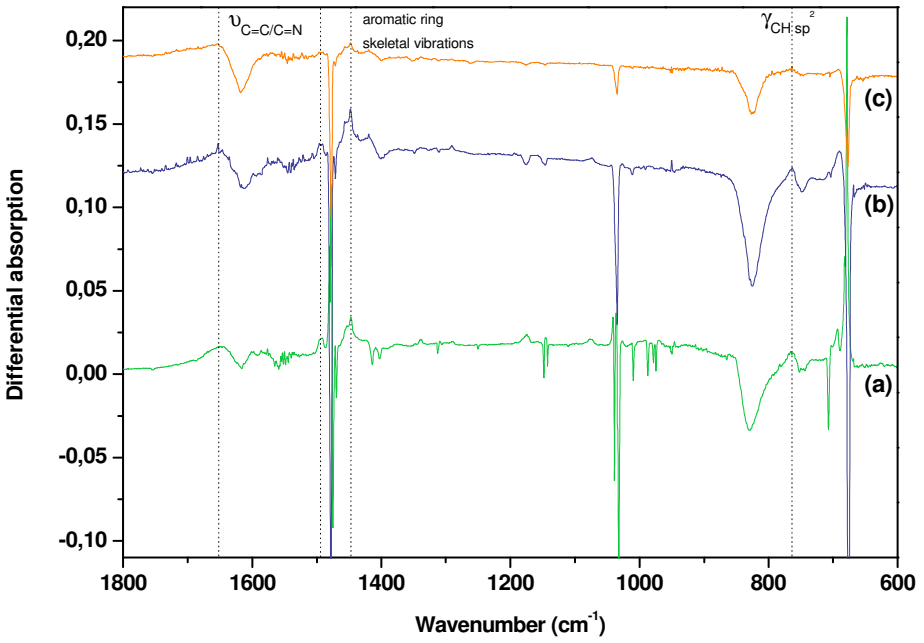

283

284 Figure **2** - FTIR difference spectra (after - before photolysis with the mercury lamp)
285 highlighting the formation of photoproducts from C_6H_6:HCN co-condensed ices at 70K : (a)
286 ratio 4:1 ; (b) ratio 1:1 ; (c) ratio 1:4. Dot lines correspond to common newly produced
287 structures.
288

289

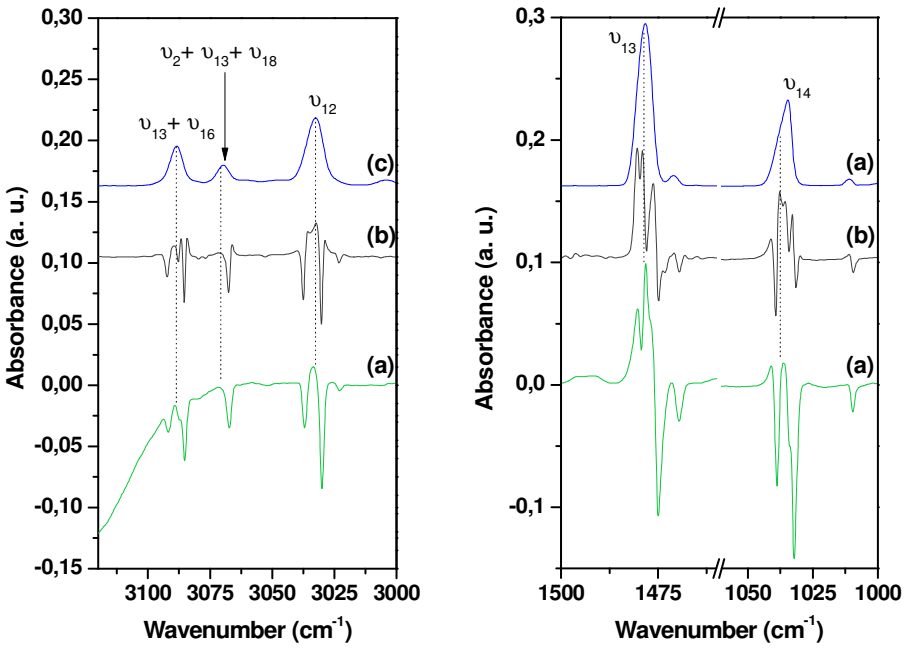

290

291 Figure **3** – Comparison of the FTIR difference spectrum after-before irradiation (with the
292 mercury lamp, 70 K) of a co-condensed ice C_6H_6:HCN 4:1 (a) and a pure benzene ice (b) with
293 the FTIR spectrum of a an amorphous benzene ice (50 K, c)
294

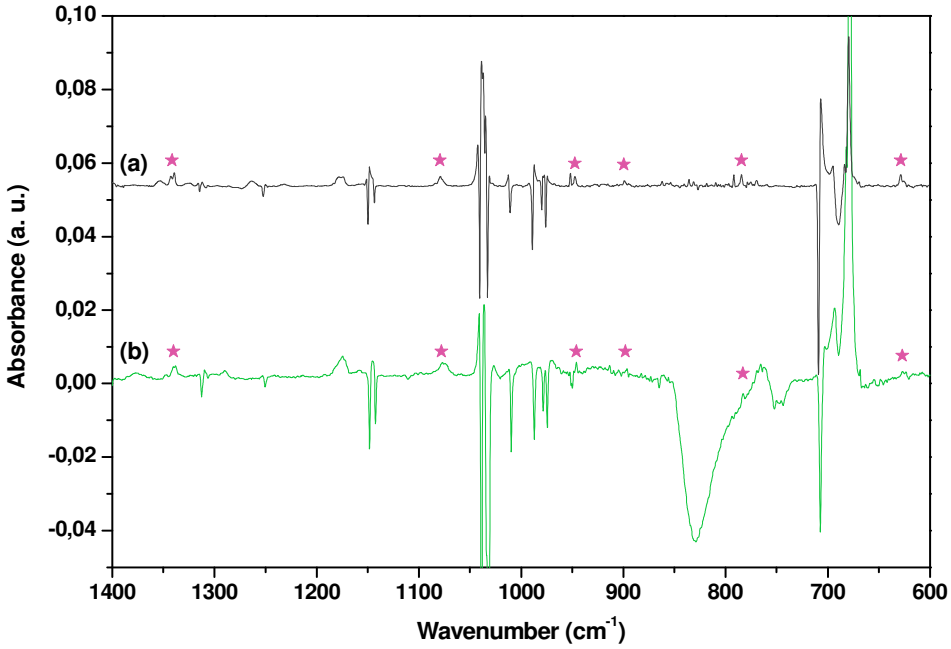

295

296 Figure **4** – Comparison of the FTIR difference spectrum after-before irradiation (with the
297 mercury lamp, 70 K) of a pure benzene ice (a) and a C_6H_6:HCN 4:1 ice (b) on which the
298 absorption bands assigned to fulvene are identified by stars
299

300

2.1.Identification of chemical functions produced by photolysis

The decrease of benzene and hydrogen cyanide observed in infrared spectroscopy during the photolysis is accompanied by the apparition of new infrared features as displayed in figures **2**, **3** and **4**. Frequencies and assignments of the new spectral features are reported in table **2**.

The peaks observed between 3000 and 2800 cm^{-1} are assigned to νCH aliphatic stretching modes. In all ices, a common maximum is observed at ~2966 and 2936 cm^{-1}, assigned to νCH_3 and νCH_2 asymmetric stretching modes (Imanaka et al. 2004; Sciamma-O'Brien et al. 2017). The shoulder at 2877 cm^{-1}, also common to all ratios can be assigned to νCH_3 symmetric stretching modes (Sciamma-O'Brien et al. 2017). The νCH aromatic stretching modes are not observed around 3100 cm^{-1} because of benzene absorption bands that mask this spectral region (figure **2**).

In other spectral regions new absorption bands are observed, which confirms the formation of structures possessing aliphatic and/or aromatic CH groups. Indeed, peaks observed at 1447 cm^{-1} and 1453 cm^{-1} (figure **2**) could both correspond to either skeletal vibration of an aromatic ring or a $-CH_3$ antisymmetric bending mode or $-CH_2$ scissor in-plane bending of aliphatic/aromatic structures (Sciamma-O'Brien et al. 2017). In all ice ratios, there is a 763 cm^{-1} peak that can be attributed to a sp^2 aromatic CH out-of-plane bending (quartet) (Carpentier et al. 2012).

The presence of nitrogenous functions can be assigned to two different bands of infrared spectra. The first bands at 3379 cm^{-1} observed in the 1:1 mix, and presumed in the others, would involves compounds with amine functions, corresponding either to $-NH_2$ asymmetric or to -NH stretching modes (Imanaka et al. 2004). The second band around 2240 cm^{-1}, with two shoulders (located at 2244 and 2231 cm^{-1}), highlitghts the formation of nitrile functions. These features can be assigned to -C≡N stretching modes of aliphatic and aromatic nitriles respectively (Carrasco et al. 2018; Sciamma-O'-Brian et al. 2017). At lower frequencies, the growth of the broad band near 2145 cm^{-1} is characteristic of isonitrile functions (Carrasco et al. 2018). Shouldered to the infrared feature of the νCN stretching mode of HCN, a new band increases around 2085 cm^{-1} in the three ices. As already observed in the case of HCN adsorbed on HC_3N photolysis, this band can be assigned to the formation of cyano-based polymeric material (Couturier-Tamburelli et al. 2018a). In addition, the common band around

1650 cm^{-1} in the three mixes can be assigned to νC=C stretching mode of alkene/aromatic structures or νC=N from imines derivatives (Sciamma-O'-Brian et al. 2017).

2.2.Identification of nitriles derivatives compounds

The analysis of infrared spectra recorded during the photolysis of C_6H_6:HCN ices show the formation of nitriles (aromatic and aliphatic) due to the appearance of a broad band between 2270 and 2210 cm^{-1}, characteristic of an overlap of several absorption bands.

Acetonitrile, propionitrile, acrylonitrile and benzonitrile are specifically targeted because they have been detected in Titan's atmosphere, except for benzonitrile which formation is only foresee by photochemical models (Loison et al. 2019). However, its detection would be the evidence of the chemical reaction between C_6H_6 and HCN in photolyzed ices. The comparison of the infrared spectra resulting from each of these targeted molecules with the difference spectrum after-before irradiation of the C_6H_6:HCN 4:1 ice is displayed in figure **5**. Infrared spectra related to the νC≡N stretching mode dominated nitrile ices. Hence, if these nitriles are formed during the photo-processing of these ices, the intensity of the νC≡N mode will be the most intense among the other modes. It is important to highlight that other nitriles derivatives, which are unknown yet, could been formed and could contribute to the spectral feature displayed in figure **5**. Frequencies of reference spectra of nitrile derivatives are also reported in table **3** and compared to the ones produced during the photo-processing of the C_6H_6:HCN 4:1 ice.

The photo-produced absorption bands at 1491, 1447 and 1289 cm^{-1} are in good agreement with the ones of the IR spectrum of a benzonitrile ice. Other spectral features of photo-produced could correspond to those of solid benzonitrile. However, they are located in spectral regions that reflect the polymerization of benzene, so their assignment is therefore not possible. Other bands are also observed and do not correspond to the ones of benzonitrile, as reported in table **3**, indicating the formation of other nitrogen-bearing derivatives. Indeed, all the absorption bands of acetonitrile were observed especially the one at 1452 cm^{-1} which cannot be attributed to any of the three previous nitriles mentioned. However, below 1700 cm^{-1}, acrylonitrile and propionitrile possess few spectral features that present weak intensities. Moreover, the figure **5** suggests that the contribution of acrylonitrile is weak from the subtraction spectrum obtained after photolysis. Its comparison with the ones of propionitrile and acrylonitrile shows a good correlation but does not allow to unambiguously confirm their formation during the photolysis process.

366

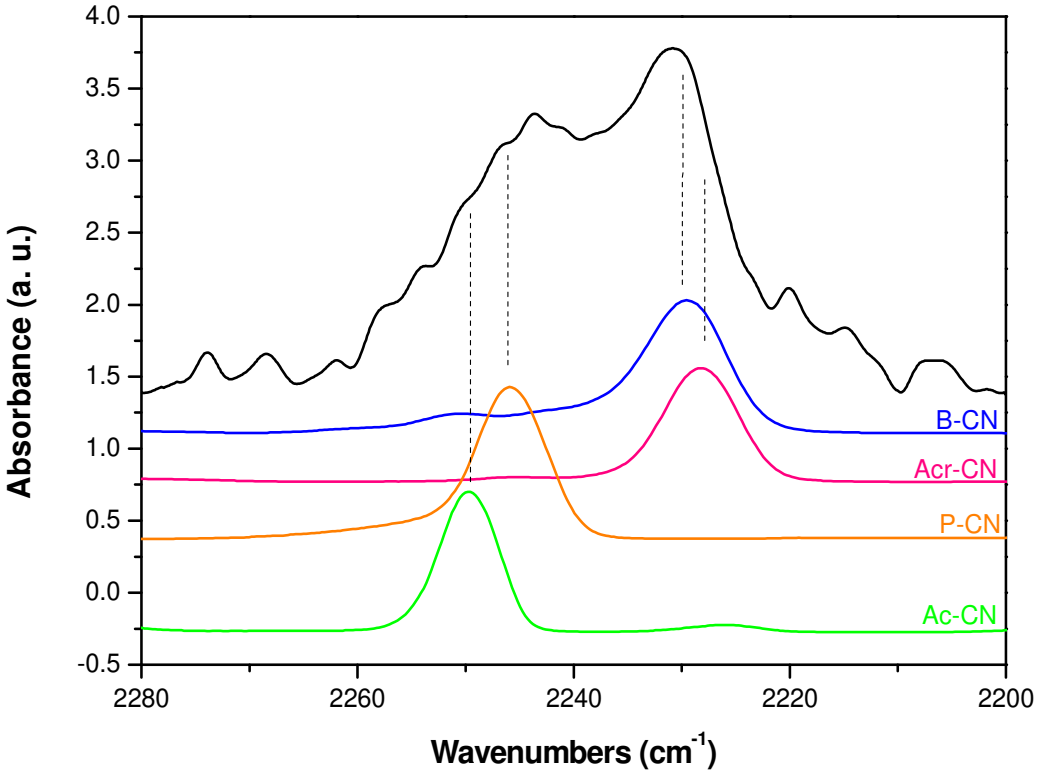

367

368

369

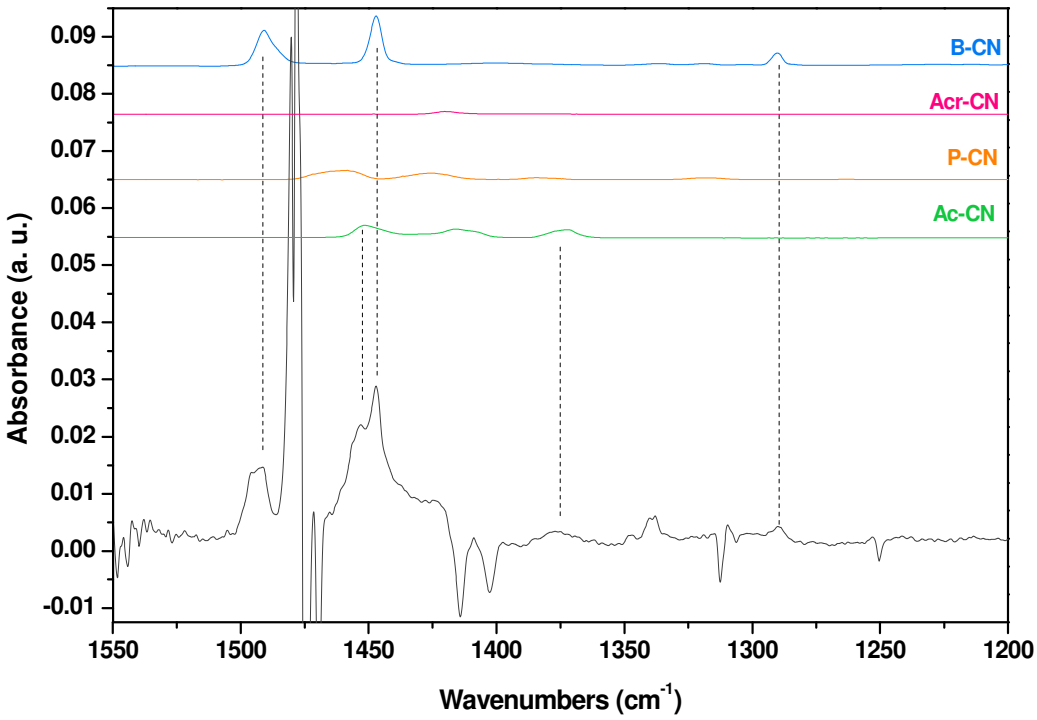

Figure **5** - Comparison between FTIR difference spectrum (after - before photolysis with mercury lamp) (multiplied by a factor 4) from C_6H_6:HCN 4:1 co-condensed ice at 70 K (black) and the infrared spectra of solid acetonitrile (Ac-CN, green), propionitrile (P-CN, orange), acrylonitrile (Acr-CN, pink) and benzonitrile (B-CN, blue).

III. Identification of volatile organic compounds by GC-MS analyses

To obtain a better identification of volatile organic compounds (VOC) formed during photolysis experiments, the C_6H_6:HCN ices were warmed up to 300 K to trap and identify by VOC GC-MS. Unfortunately, we cannot rule out that during the annealing, other products than those formed in the solid phase during the photolysis process may be formed. However, the chromatographic experiments should allow us to confirm the formation of products identified by IR spectroscopy and to determine if these products are identical in the three ice ratio. The three TIC (Total Ion Current) chromatograms (figure **6**) correspond to the three experiments, the ratio 4:1, 1:1 and 1:4 of C_6H_6:HCN ices, submitted to long-UV radiations and subsequently warmed. The identification of the VOC are realized thanks to the injection of standards in the same analytical conditions used for the analyzes of the gas phase of photo-processed C_6H_6:HCN ices. Three parameters from the TIC chromatograms allow the identification of organic compounds which are the concordance of retention times, mass fragmentation patterns as well as the presence of a mass shift related to the number of

nitrogen atoms in the N^{15} experiments. The identification of hydrocarbons is based on the comparison with the GC-MS analyses of the photo-processing of pure benzene ($^{12/13}C_6H_6$) ices (Mouzay et al., 2021b).

The peaks labelled from I to V correspond respectively to hydrogen cyanide, acetonitrile, propionitrile, acrylonitrile and benzonitrile which confirm their identification obtained with infrared spectroscopy after the photolysis process (cf. figures **S2-S5**, supplementary information). Hydrocarbons already detected in the gas phase after the photoprocessing of a pure benzene ice (Mouzay et al. 2021b) are also identified in the gas phase of C_6H_6:HCN ices (labels 1-18). In relation to the IR spectra recorded during the photolysis experiment (cf. figure **2**), absorption bands, observed after the photo-processing of C_6H_6:HCN ices at 1447 and 1453 cm^{-1} could be attributed to the formation of these volatile aromatic derivatives (νC=C stretching modes), based on Sciamma O'Brien et al.'s work (2017).

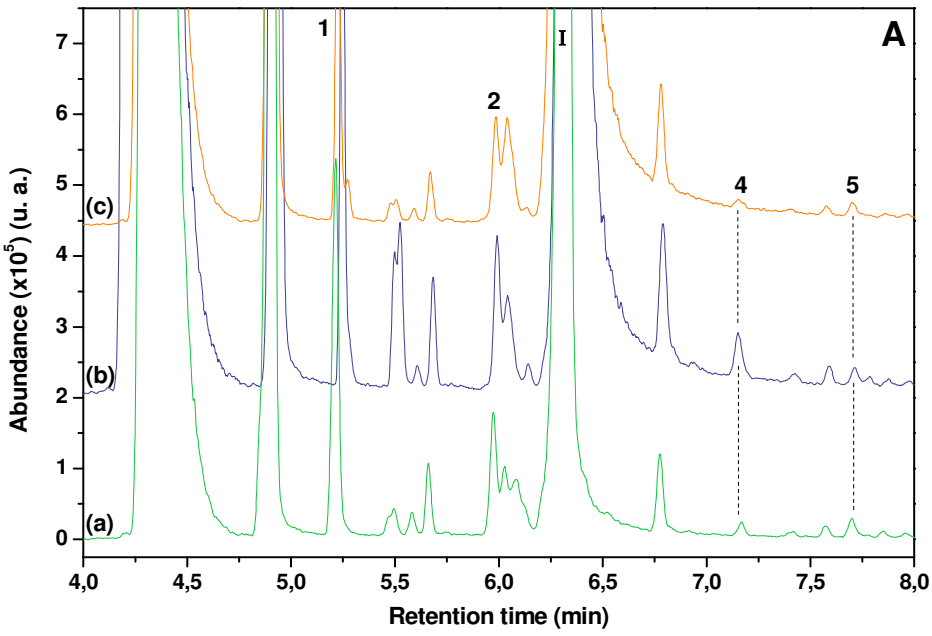

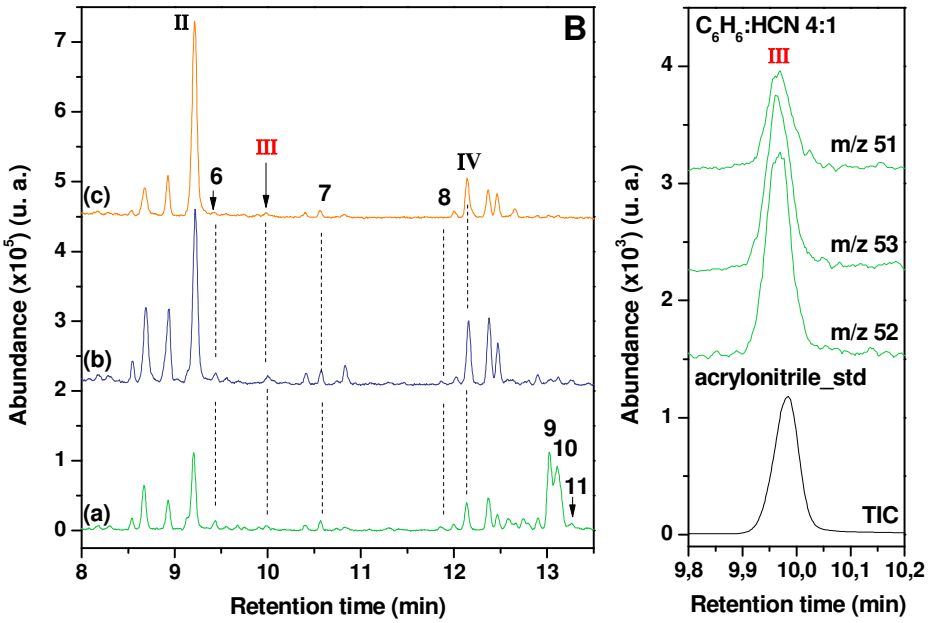

404

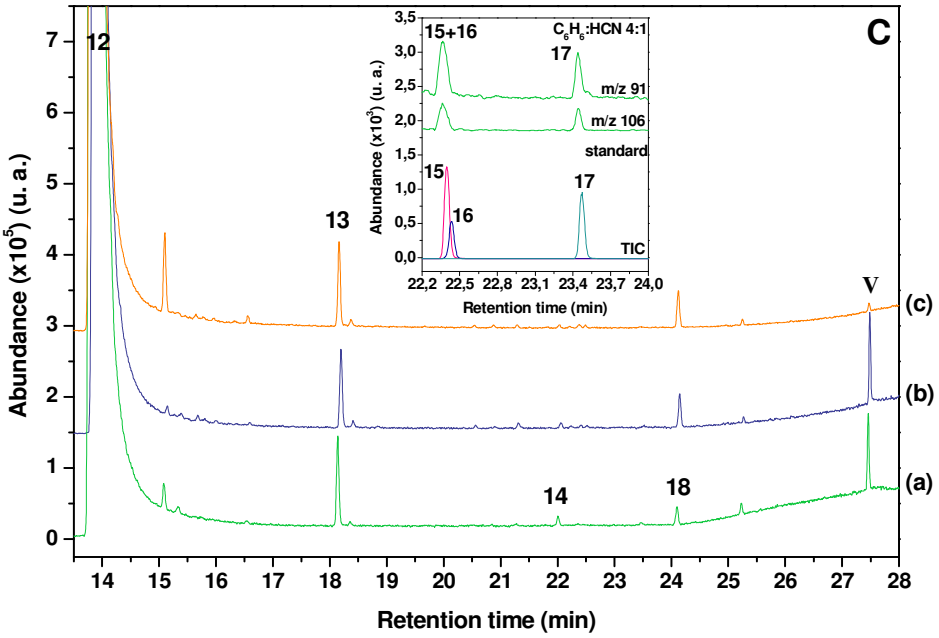

405

406 Figure **6** - (A-B-C) TIC GC-MS chromatograms of the gas phases released during the
407 warming-up of photo-processed with mercury lamp C_6H_6:HCN co-condensed ices in a ratio
408 4:1 (a), 1:1 (b) and 1:4 (c). The enlarged part (B) displays the ion extracted chromatogram of
409 the three most intense fragment of acrylonitrile (bottom part) compared to the TIC
410 chromatogram of the corresponding standard (top part). The enlarged part (C) displays the ion
411 extracted chromatogram of the two most intense fragments of xylene isomers (top part) and
412 are compare to the TIC chromatogram of the corresponding standard (bottom part) o-xylene,
413 m-xylene and p-xylene. The peak at 22.4 min (15+16) corresponds to the co-elution of m- and
414 p-xylene.
415

416

Discussion and conclusion

The formation and the composition of Titan's stratospheric ice clouds are the result of complex processes within the framework of observations performed on the solar system's bodies. Many works inferred the presence of nitrile species like HCN, HC_3N, CH_3CN, in the upper atmosphere which diffuse to lower altitudes, while they are submitted to long-UV photons. These molecules potentially lead to the formation of aerosols by condensation (Sciamma O'Brien et al.'s work 2017). Anderson et al (2017) reported the detection of massive cloud around 250 km of altitude. Experimental simulation indicates that the CIRS-detected HASP cloud's chemical composition is consistent with a C_6H_6:HCN ice containing ~ approximatively 80% C_6H_6 and 20% HCN (Anderson et al 2017).

In this work, we aimed to simulate the photochemical aging in the stratosphere of benzene condensed simultaneously with hydrogen cyanide. From the results obtained after the photolysis of C_6H_6:HCN ices, at 70 K, with a mercury lamp, dynamic organic chemistry has been demonstrated. Thanks to IR spectroscopy, we identified in solid phase benzonitrile and acetonitrile and we proposed as tentative attempt propionitrile and acrylonitrile molecules. Through the identification of these nitrile derivatives, we demonstrated a solid-state consumption pathway relevant for Titan's stratospheric chemistry, triggered by the photochemical activation of C_6H_6. These results demonstrated the possibility of a solid-state formation pathway of nitrile derivatives from the photo-processing of different C_6H_6:HCN ices and by extension from the CIRS-HASP cloud. As first mentioned theoretically by Anderson et al. (2016), stratospheric clouds could thus participate to the formation of complex molecules referring to this experimental work. Of course, the results obtain in this study must be taken cautiously because we simulate a simplified thin cloud exposed during 2.6 years while the timescale on Titan are higher. Moreover, the thickness of the cloud is not taken into account in our experimental work and the photochemical reactivity studied can only affect the first layers of the cloud. We have also to take in mind that the surface of the cloud is regularly renewed so that molecules detected here might be formed in different quantities on Titan.

The temperature of Titan's stratosphere varies from 70 to 190 K at 79°S in July 2015 (Anderson et al 2018). To take into account the warming-up of the stratosphere reported by Coustenis et al. (2019) in the region in which the HASP cloud has been detected, we performed a slow warming-up of the irradiated ices, formed by co-condensation processes. Of course, because of our experimental constraints, the warming is performed up to room temperature which is much higher than those reached in the Titan atmosphere Hence, this step

allows to determine the role of the UV-Vis radiations-induced photochemical aging in the potential formation of volatile photo-products in Titan's stratosphere. From the GC-MS analyses performed on the volatile fraction that has sublimated from these photo-processed ices, we confirmed the formation of acrylonitrile (Cui et al. 2009; Lellouch et al. 2010; Magee et al. 2009) and acetonitrile (Cui et al. 2009) which have been detected in gas phase in Titan's stratosphere. Mixing ratio of acetonitrile has been estimated to be 10^{-8} at 200 km (Nixon et al. 2010 against 10^{-9} for acrylonitrile and propionitrile (Cordiner at al. 2015; Marten 2002; Palmer et al. 2017). In addition, we have identified benzonitrile that has not been detected yet in Titan's atmosphere by IR spectroscopy (VIMS/CIRS instruments) or mass spectrometry (INMS instrument). Its only astrophysical detection to date has taken place in the interstellar medium (McGuire et al. 2018). In the stratosphere (around 200 km) according to the photochemical model (radiative transfer) developed by Loison et al. (2019), benzonitrile formation could result from the direct bimolecular reaction involving CN radical with benzene. Therefore, this production in the lower atmospheric layers is weak since CN are very efficiently consumed through reactions with CH_4. Despite a strong dipole moment, its weak abundance at these altitudes will make the benzonitrile detection difficult (Loison et al. 2019). In addition, hydrocarbons coming from the photo-degradation of benzene have been detected and their production rates seem to be affected by the mixing ratio of the initial ice. An exhaustive analysis of this effect will require additional experiments and will be investigated in the future. However, our laboratory experiments demonstrate for the first time that the massive HASP icy cloud's chemical composition could potentially be a source of a rich production of this aromatic nitrile, among other nitriles derivatives or hydrocarbons. These molecules might be released in gas phase in the stratosphere, when changing season occurs, as observed at the south pole (Coustenis et al. 2019). These organics will probably diffuse towards lower altitudes until they reach the surface. Hence, this work demonstrates the importance of laboratory experiments to prepare future space missions, in particular the Dragonfly space mission dedicated to the analysis of the organic layer that recovers Titan's lakes and ground. It provides a list of molecules that may be detected during this future mission. Moreover, the results brought by this experimental work could supply motivating elements for future space missions dedicated in part to the specific study of the chemistry of stratospheric clouds, as reported by Nixon et al. (2020).

Acknowledgements

This work has been funded by the French national program “PNP”, Programme de Physique et Chimie du Milieu Interstellaire (PCMI, INSU), and the Centre National d’Etudes Spatiales (CNES, exobiology program). It was also supported by the French Agence Nationale de la Recherche (VAHIIA grant ANR-12-JS08-0001 and RAHIA_SSOM grant ANR-16-CE29-0015).

References

Abou Mrad, N., Duvernay, F., Chiavassa, T., & Danger, G. 2016, Mon Not R Astron Soc, 458, 1234

Abou Mrad, N., Duvernay, F., Theulé, P., Chiavassa, T., & Danger, G. 2014, Anal Chem, 86, 8391

Abou Mrad, N., Werner, S., Mouzay, J., & Danger, G. 2020, J Chromatogr A, 1609, 460489

Abplanalp, M. J., Góbi, S., & Kaiser, R. I. 2019, Phys Chem Chem Phys, 21, 5378

Achterberg, R. K., Gierasch, P. J., Conrath, B. J., et al. 2014, in AAS/Division for Planetary Sciences Meeting Abstracts#46, Vol. 46

Anderson, C. M., Samuelson, R. E., & Nna-Mvondo, D. 2018, Space Sci Rev, 214, http://link.springer.com/10.1007/s11214-018-0559-5

Anderson, C. M., Samuelson R. E., Yung Y. L., & McLain J. L. 2016, Geophys Res Lett, 43, 3088

Anderson, C., Nna-Mvondo, D., Samuelson, R. E., et al. 2017, Vol. 49, 304.10, http://adsabs.harvard.edu/abs/2017DPS....4930410A

Barth, E. L. 2017, Planet Space Sci, 137, 20

Bernstein, M. P., Sandford, S. A., & Allamandola, L. J. 1997, Astrophys J, 476, 932

Bertie, J. E., & Keefe, C. D. 2004, J Mol Struct, 695–696, 39

Butscher, T., Duvernay, F., Theule, P., et al. 2015, Mon Not R Astron Soc, 453, 1587

Carpentier, Y., Féraud, G., Dartois, E., et al. 2012, Astron Astrophys, 548, A40

Carrasco, N., Tigrine, S., Gavilan, L., Nahon, L., & Gudipati, M. S. 2018, Nat Astron, http://www.nature.com/articles/s41550-018-0439-7

Clarke, D. 2000, Icarus, 147, 282

Coates, A. J., Wellbrock, A., Lewis, G. R., et al. 2009, Planet Space Sci, 57, 1866

Coll, P., Coscia, D., Smith, N., et al. 1999, Planet Space Sci, 47, 1331

Cordiner, M. A., Palmer, M. Y., Nixon, C. A., et al. 2015, Astrophys J, 800, L14

Coustenis, A., Achterberg, R. K., Conrath, B. J., et al. 2007, Icarus, 189, 35

Coustenis, A., Jennings, D. E., Achterberg, R. K., et al. 2016, Icarus, 270, 409

Coustenis, A., Jennings, D. E., Achterberg, R. K., et al. 2019, Icarus

Coustenis, A., Salama, A., Schulz, B., et al. 2003, Icarus, 161, 383

517 Coustenis, A., Schmitt, B., Khanna, R. K., & Trotta, F. 1999, Planet Space Sci, 47, 1305

518 Couturier-Tamburelli, I., Gudipati, M. S., Lignell, A., Jacovi, R., & Piétri, N. 2014, Icarus, 234, 81

519 Couturier-Tamburelli, I., Piétri, N., Letty, V. L., Chiavassa, T., & Gudipati, M. 2018a, Astrophys J,
520 852, 117

521 Couturier-Tamburelli, I., Toumi, A., Piétri, N., & Chiavassa, T. 2018b, Icarus, 300, 477

522 Cui, J., Yelle, R. V., Vuitton, V., et al. 2009, Icarus, 200, 581

523 Dawes, A., Pascual, N., Hoffmann, S. V., Jones, N. C., & Mason, N. J. 2017, Phys Chem Chem Phys,
524 19, 27544

525 De Kok, R., Irwin, P., Teanby, N., et al. 2007, Icarus, 191, 223

526 Fleury, B., Gudipati, M. S., Couturier-Tamburelli, I., & Carrasco, N. 2019, Icarus, 321, 358

527 Galand, M., Yelle, R., Cui, J., et al. 2010, J Geophys Res Space Phys, 115

528 Gautier, T., Carrasco, N., Buch, A., et al. 2011, Icarus, 213, 625

529 Gerakines, P. A., Moore, M. H., & Hudson, R. L. 2004, Icarus, 170, 202

530 Griffith, C. A., Penteado, P., Rannou, P., et al. 2006, Science, 313, 1620

531 Gudipati, M. S., Jacovi, R., Couturier-Tamburelli, I., Lignell, A., & Allen, M. 2013, Nat Commun, 4,
532 1648

533 Hanel, R., Conrath, B., Flasar, F. M., et al. 1981, Science, 212, 192

534 Hodyss, R., Johnson, P. V., Orzechowska, G. E. et al. 2008, Icarus, 194, 836

535 Hörst, S. M., Yoon, Y. H., Ugelow, M. S., Parker, A. H., & Li, R. 2018, Icarus, 301, 136

536 Imanaka, H., Khare, B. N., Elsila, J. E., et al. 2004, Icarus, 168, 344

537 Imanaka, H., & Smith, M. A. 2007, Geophys Res Lett, 34, L02204

538 Imanaka, H., & Smith, M. A. 2010, Proc Natl Acad Sci, 107, 12423

539 Jacovi, R., Laufer, D., Dimitrov, V., & Bar-Nun, A. 2010, J Geophys Res Planets, 115, E07006

540 Khanna, R. K., Perera-Jarmer, M. A., & Ospina, M. J. 1987, Spectrochim Acta Part Mol Spectrosc, 43,
541 421

542 Koskinen, T. T., Yelle, R. V., Snowden, D. S., et al. 2011, Icarus, 216, 507

543 Kunde, V. G., Aikin, A. C., Hanel, R. A., et al. 1981, Nature, 292, 686

544 Lavvas, P., Griffith, C. A., & Yelle, R. V. 2011, Icarus, 215, 732

545 Lavvas, P. P., Coustenis, A., & Vardavas, I. M. 2008, Planet Space Sci, 56, 67

546 Lavvas, P., Yelle, R. V., & Griffith, C. A. 2010, Icarus, 210, 832

547 Lellouch, E., Vinatier, S., Moreno, R., et al. 2010, Planet Space Sci, 58, 1724

548 Lignell, A., Gudipati, M. S. 2015, J. Phys. Chem. A, 119, 11, 2607.

549 Loison, J. C., Dobrijevic, M., & Hickson, K. M. 2019, Icarus, 329, 55

550 Magee, B. A., Waite, J. H., Mandt, K. E., et al. 2009, Planet Space Sci, 57, 1895

551 Mair, R. D., & Hornig, D. F. 1949, J Chem Phys, 17, 1236

552 Marten, A. 2002, Icarus, 158, 532

553 Mateus, M. P. S., Galamba, N., & Cabral, B. J. C. 2011, J Phys Chem A, 115, 13714

554 Mayo, L., & Samuelson, R. 2005, Icarus, 176, 316

555 McGuire, B. A., Burkhardt, A. M., Kalenskii, S., et al. 2018, Science, 359, 202

556 Mouzay, J., Couturier-Tamburelli, I., Piétri, N., & Chiavassa, T. 2021a, J Geophys Res Planets, 126,
557 e2020JE006566, https://doi.org/10.1029/2020JE006566

558 Mouzay, J., Henry, K., Ruf, A., I. Couturier-Tamburelli, I., Danger, G., Piétri, N., Chiavassa, T.
559 2021b, 2021 Planet. Sci. J., 2 , 37

560 Mouzay, J., Piétri, N., Couturier-Tamburelli, I., Chiavassa, T. 2021c, J. mol. Struct. 1237, 130296

561 Mutsukura, N., & Akita, K. 1999, Thin Solid Films, 5

562 Navarro-González, R., Ramírez, S. I., de la Rosa, J. G., Coll, P., & Raulin, F. 2001, Adv Space Res,
563 27, 271

564 Niemann, H. B., Atreya, S. K., Demick, J. E., et al. 2010, J Geophys Res, 115, E12006,
565 doi:10.1029/2010JE003659.

566 Nixon, C. A., Abshire, J., Ashton, A., et al. 2020, ArXiv200805680 Astro-Ph

567 Nixon, C. A., Achterberg, R. K., Irwin, P. G. J., et al. 2010, Faraday Discuss, 147, 65

568 Palmer, M. Y., Cordiner, M. A., Nixon, C. A., et al. 2017, Sci Adv, 3, e1700022

569 Pola, J., Ouchi, A., Maryško, M., et al. 2011, J Photochem Photobiol Chem, 220, 188

570 Ramírez, S. I., Navarro-González, R., Coll, P., & Raulin, F. 2001, Adv Space Res, 27, 261

571 Ramírez, S. I., Navarro-González, R., Coll, P., & Raulin, F. 2005, Adv Space Res, 36, 274

572 Samuelson, R. E., & A. Mayo, L. 1991, Icarus, 91, 207

573 Samuelson, R. E., Nath, N. R., & Borysow, A. 1997, Planet Space Sci, 45, 959

574 Samuelson, R. E., Smith, M. D., Achterberg, R. K., & Pearl, J. C. 2007, Icarus, 189, 63

575 Sciamma-O'Brien, E., Upton, K. T., & Salama, F. 2017, Icarus, 289, 214

576 Strazzulla, G., & Baratta, G. A. 1991, Astron Astrophys, 241, 310

577 Torokova, L., Watson, J., Krcma, F., et al. 2015, Contrib Plasma Phys, 55, 470

578 Toumi, A., Piétri, N., Chiavassa, T., & Couturier-Tamburelli, I. 2016, Icarus, 270, 435

579 Tran, B. N., Joseph, J. C., Force, M., et al. 2005, Icarus, 177, 106

580 Vinatier, S., Schmitt, B., Bezard, B., et al. 2018, Icarus, 310, 89

581 Waite, J. H., Niemann, H., Yelle, R. V., et al. 2005, Science, 308, 982

582 Waite, J. H., Young, D. T., Cravens, T. E., et al. 2007, Science, 316, 870

583 Wilson, E. H. 2004, J Geophys Res, 109, http://doi.wiley.com/10.1029/2003JE002181

584 Yung, Y. L., Allen, M., & Pinto, J. P. 1984, Astrophys J Suppl Ser, 55, 465

585 **Table 1**

586 Positions, assignments and band strength of infrared absorption bands of C_6H_6 and HCN in the co-condensed ices at 70 K after annealed to 105 K

	Assignments [a, b]	**Wavenumbers (cm^{-1})**					
		This work			Mouzay et al. (2021a)		This work
		C_6H_6:HCN 4:1	**C_6H_6:HCN 1:1**	**C_6H_6:HCN 1:4**	**Pure C_6H_6 ice (70 K after annealing)**	**Pure C_6H_6 ice (amorphous)**	**Pure HCN ice (70 K after annealing)**
C_6H_6	$\nu_{13} + \nu_{16}$, e_{1u} CH aromatic stretching	3092 3086	3089	3090	3091 3084	3088	-
	$\nu_2 + \nu_{16} + \nu_{18}$, e_{1u}	3068	3070	3071	3067	3070	-
	ν_{12}, e_{1u}	3037 3030	3034	3035	3036 3029	3032	-
	ν_{13}, e_{1u} C=C aromatic stretching	1478 1475	1478	1478	1477 1474	1477	-
	ν_{14}, e_{1u} C-H in-plane bending	1039 1032	1034	1035	1038 1032	1034	-
	ν_4, a_{2u} C-H out of plane bending	679	676	678	680	674	-
HCN	ν_1, Σ^+, CH stretching	3126	3124	3137	-	-	3121
	ν_2, Σ^+, C≡N stretching	2101	2101	2100	-	-	2097
	$2\nu_3$, π	1616	1618	1622	-	-	1625
	ν_3, π, CH bending	829	828	828	-	-	826
C_6H_6:HCN	$C_{sp}H$ stretching	3210	3202	3202	-	-	-

587 [a] Bertie & Keefe, 2004; Mair & Hornig, 1949 ; [b] Bernstein et al. 1997; Gerakines et al. 2004

Table 2

Positions, assignments of new infrared absorption bands obtained during the photolysis at 70 K of C_6H_6:HCN mixes (λ > 230nm)

Assignments	Wavenumbers (cm^{-1}) This work C_6H_6:HCN 4:1	Wavenumbers (cm^{-1}) This work C_6H_6:HCN 1:1	Wavenumbers (cm^{-1}) This work C_6H_6:HCN 1:4	References
asymmetric stretching -NH_2/-NH- stretching	3353	3379	3355	a
asymmetric stretching CH_3	2966	2966	2966	a, b
asymmetric stretching CH_2	2936	2936	2935	a, b
symmetric stretching CH_3	2877	2877	2877	a, b
–C≡N stretching (aliphatic nitriles)	2244	2244	2246	a, c, d
–C≡N stretching (aromatic nitriles)	2231	2232	2237	a, d
–N≡C stretching (aliphatic isonitriles)	2143	2146	2140	c, d
C=C stretching (alkene/aromatics)/C=N stretching (imines)	1653	1653	1653	b
C=C stretching (alkene/aromatics)/	1600-1565	1598-1550	1590-1550	
aromatic ring skeletal vibration	1491	1491	1491	b, e
aromatic ring skeletal vibration and –CH_3 (as) bending/–CH_2 scissor in plane bending (alkane/aliphatic and aromatic)	1453	1457	1457	b, e
aromatic ring skeletal vibration and –CH_3 (as) bending/–CH_2 scissor in plane bending (alkane/aliphatic and aromatic)	1447	1448	1447	b
νC-N stretching (aromatic amines)	1289	1290	-	b
in plane bending =CH (alkene/aromatic)/ νC-N	1073	1073	-	b
out of plane bending –CH sp^2 (aromatic)	798-754	798-754	-	b, e

References

[a] Imanaka et al. 2004 ; [b] Sciamma-O'Brien et al. 2017 ; [c] Carrasco et al. 2018 ; [d] Mutsukura & Akita 1999 ; [e] Strazzulla & Barata

Table 3

Experimental new infrared bands obtained during the photolysis of C_6H_6:HCN (4:1) mix compared with those of nitriles ice recorded at 70 K

Acetonitrile CH_3CN	**Propionitrile** C_2H_5CN	**Acrylonitrile** C_2H_3CN	**Benzonitrile** C_6H_5CN	**C_6H_6:HCN 4:1**
	2952			2966
2940				2936
	2890			2877
2248	2245			2278-2212
		2227	2231	
			1598	
			1582	1600-1565
			1572	
			1489	1491
1452	1460*			1453
			1445	1447
	1425			1424
1415*		1413*		
	1316*			
			1289	1289
			1192*	
			1178*	
			1161*	
	1074		1072	1073
1037*				
			1026*	
	1003*	976*		
916				
771	782	759	758	795-754

* absorption bands masked by the IR features of benzene.

Table 4 – List of volatile photoproducts identified by GC-MS - coming from the photo-processing of co-condensed ices C_6H_6:HCN 4:1/1:1/1:4 at 70 K subsequently warmed-up to 300 K. The comparison with identifications reported in the literature is also mentioned.

Products identified		Peak identification	Identification	Detected in laboratory experiments	
				High altitude conditions	Low altitude conditions
C3	propene (C_3H_6)	1	NIST	b,f,c,d,e,f	g, i
C4	but-2-ene (C_4H_8)	2	NIST	a,b,c,e	g
	but-1-en-3-yne (C_4H_4)	3	NIST	b,c,e	g
	diacetylene (C_4H_2)	4	NIST	c,e	g, i
C5	pentane (C_5H_{12})	5	standard	a,b,c,d,f	g
	2-methyl-buta-1.3-diene (C_5H_8)	6	NIST	no	g
C6	hexane (C_6H_{14})	7	standard	a,b,c	g
	methylcyclopentane (C_6H_{12})	8	NIST	no	g
	fulvene ? (C_6H_6)	9	NIST	no	no
	C_6H_6 isomer	10	NIST	no	no
	cyclohexane (C_6H_{12})	11	standard	no	g
	benzene (C_6H_6)	12	standard	c	g
C7	toluene (C_7H_8)	13	standard	c,e	g
C8	ethylbenzene (C_8H_{10})	14	standard	no	g
	m-xylene (C_8H_{10})	15+16	standard	no	g
	p-xylene (C_8H_{10})		standard	no	g
	o-xylene (C_8H_{10})	17	standard	no	g
	styrene (C_8H_8)	18	standard	no	g,h
C1	hydrogen cyanide (HCN)	I	standard	a,b,c,d,e,f	i,j
C2	acetonitrile (CH_3CN)	II	standard	a,b,c,d,e,f	h,i,i
C3	propionitrile (C_2H_5CN)	III	standard	a,b,c,d,e	h,i
	acrylonitrile (C_2H_3CN)	IV	standard	a,b,c,d,e	i,j
C7	benzonitrile (C_6H_5CN)	V	standard	no	no

References : [a] Coll et al. 1999 ; [b] Ramírez et al. 2005, 2001 ; [c] Navarro-González et al. 2001 ; [d] Gautier et al. 2011; [e] Torokova et al. 2015 ; [f] anaka & Smith, 2010 ; [g] Tran et al. 2005; [h] Jacovi et al. 2010 ; [i] Hörst et al. 2018; [j] Clarke 2000

Supplementary material

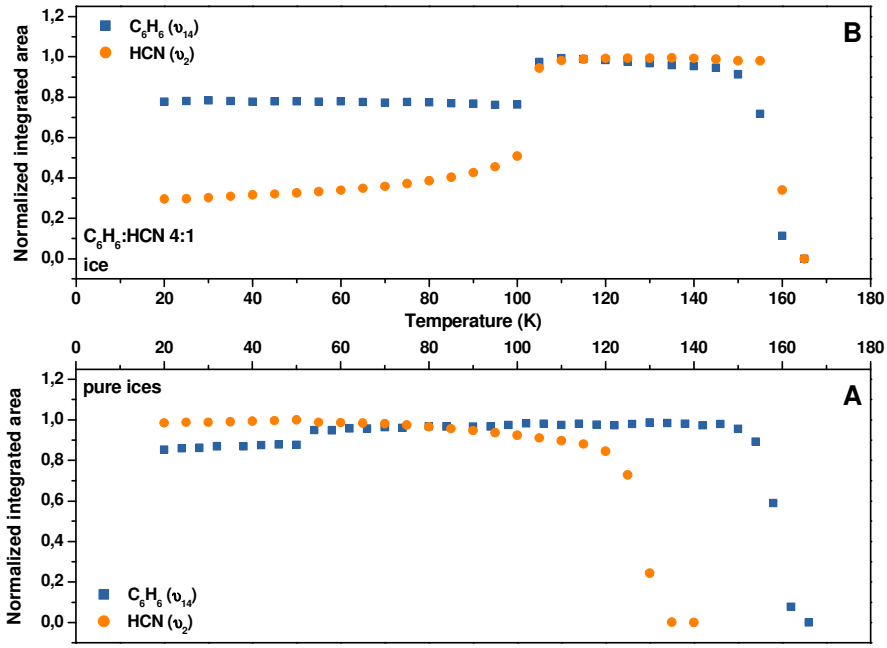

Figure **S1** - Comparison of the evolution of the normalized integrated areas of the IR absorption bands related to benzene ν_{14} and HCN ν_2 vibrational modes in: (A) in pure ices and (B) in a C_6H_6:HCN co-condensed ice (4:1 ratio), as a function of temperature (β = 1 K.min^{-1}). Each of these ices was initially deposited at 20 K and then warmed-up until complete desorption visualized by the total disappearance of their spectral features from the IR spectra recorded regularly during this step. In the case of pure ices, desorption of HCN begins as early as 80 K, while that of benzene is observed from 130 K (A). In the case of the C_6H_6:HCN co-condensed ice (B), the sublimation of benzene, started from 110 K, leads to that of HCN at 150 K. It should also be noted that the crystallization temperature is modified by this interaction as the transition from an amorphous to a crystalline phase is observed simultaneously for C_6H_6 and HCN between 100 and 105 K, against ~55 K for C_6H_6 in a pure ice.

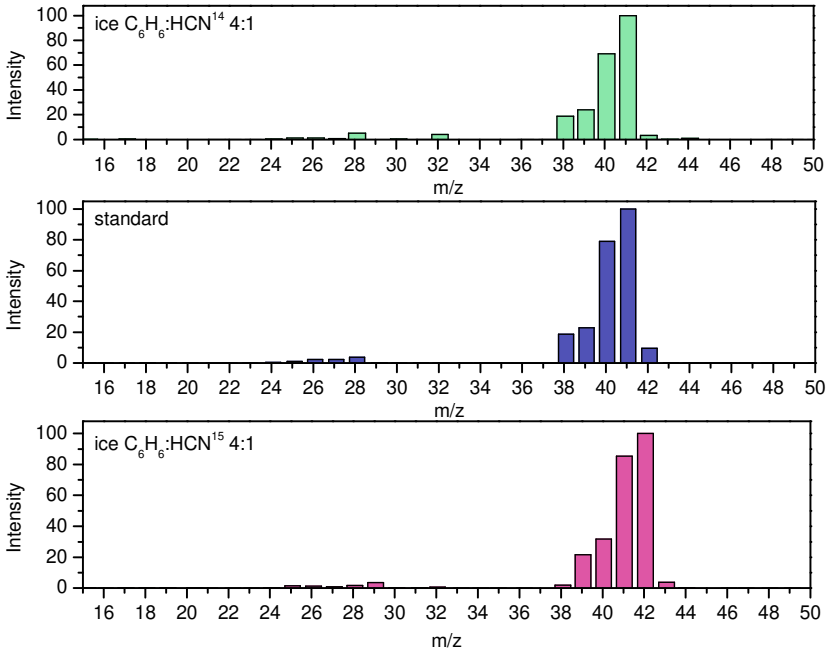

Figure **S2** - Mass spectra of acetonitrile (peak **II**) from C_6H_6:HCN^{14} 4:1 ice (top, green), standard (middle, blue) and C_6H_6:HCN^{15} 4:1 ice (bottom, pink)

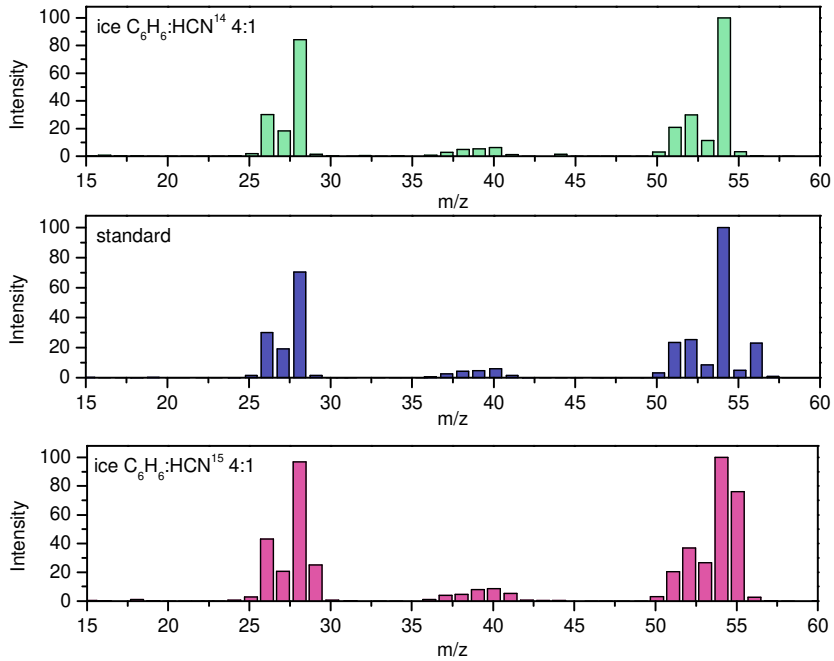

Figure **S3** - Mass spectra of propionitrile (peak **III**) from C_6H_6:HCN^{14} 4:1 ice (top, green), standard (middle, blue) and C_6H_6:HCN^{15} 4:1 ice (bottom, pink)

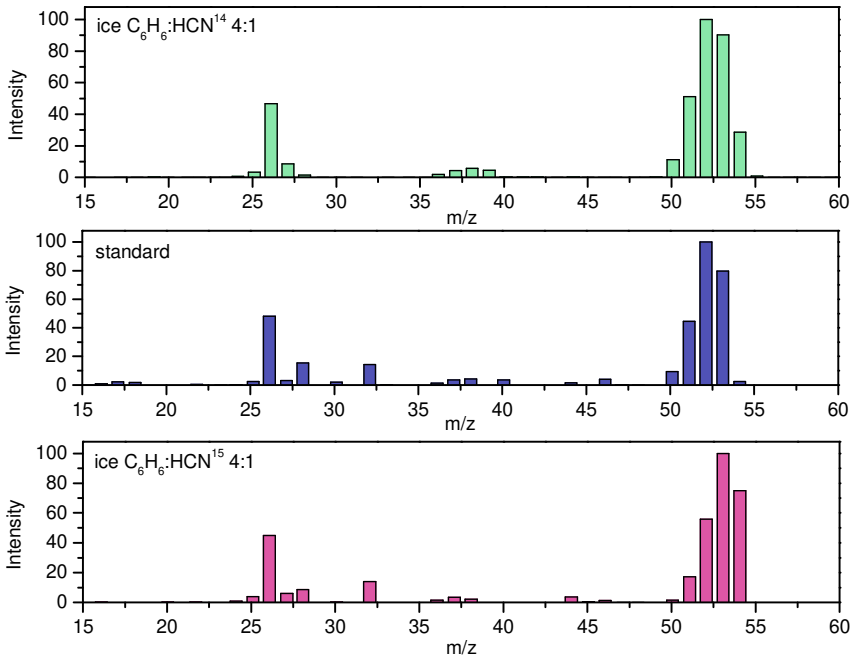

Figure **S4** - Mass spectra of acrylonitrile (peak **IV**) from C_6H_6:HCN^{14} 4:1 ice (top, green), standard (middle, blue) and C_6H_6:HCN^{15} 4:1 ice (bottom, pink)

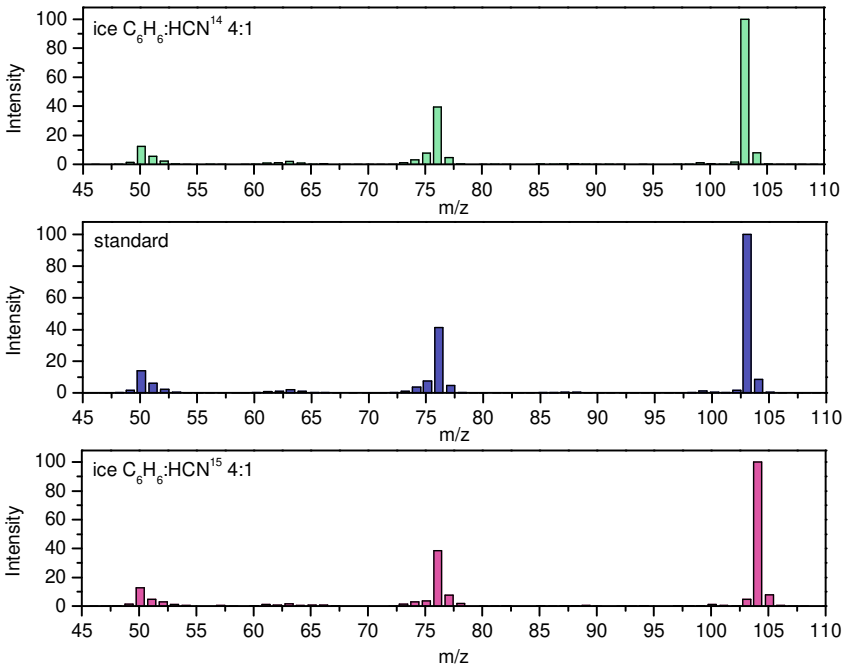

Figure **S5** - Mass spectra of benzonitrile (peak **V**) from C_6H_6:HCN^{14} 4:1 ice (top, green), standard (middle, blue) and C_6H_6:HCN^{15} 4:1 ice (bottom, pink)